Biomass and Bioenergy 199 (2025) 107936

Contents lists available at ScienceDirect

Biomass and Bioenergy

journal homepage: www.elsevier.com/locate/biombioe

# MgO-based catalysts for selective delignification of lignocellulosic waste and carboxylic acids production under mild hydrothermal conditions

N. Vidal [a,b], M. Ventura [a,b], M. Orfila [a], F. Martínez [a,b], J.A. Melero [a,b,*]

[a] Chemical & Environmental Engineering Group, Universidad Rey Juan Carlos. C/Tulipán s/n, 28933, Móstoles, Spain
[b] Instituto de Investigación de Tecnologías para la Sostenibilidad. Universidad Rey Juan Carlos. C/Tulipán s/n, 28933, Móstoles, Spain

ARTICLE INFO

*Keywords:*
Delignification
Lignocellulosic waste
(di)carboxylic acids
Catalyst
Magnesium oxide

ABSTRACT

Lignocellulosic biomass offers a sustainable alternative to traditional raw materials. However, its complex structure, and particularly the presence of lignin, presents a significant challenge for its conversion into valuable products. This study explores the catalytic performance of magnesium oxide (MgO) based materials for the selective delignification of lignocellulosic waste and concomitant carboxylic acids production. Different MgO samples have been synthesized through various synthetical methods with the purpose of promoting the selective delignification of a lignocellulose waste while minimizing the degradation of other polymers (cellulose and hemicellulose). The resultant lignin-free holocellulose solid after selective depolymerization might be used in subsequent fermentation processes. The catalytic results demonstrated that MgO synthesized by a sol-gel method exhibited the highest catalytic activity, achieving ca. 90 % lignin conversion with minimal degradation of cellulose and hemicellulose and outstanding production of carboxylic acids (ca. 30 % of the carbon of the degraded polymers was converted into carboxylic acids). The high concentration of medium-strength base sites combined with significant macroporosity are crucial for enhancing the catalytic performance of MgO-based catalysts. Importantly, these results were achieved under mild conditions (120 °C) using water as a solvent and without addition of external oxidant agents. Furthermore, the study observed a significant production of valuable (di) carboxylic acids, such as fumaric acid during the depolymerization process over optimized MgO catalyst. This research provides valuable insights into the potential of MgO as a sustainable catalyst for the selective conversion of lignin present in lignocellulosic biomass into valuable chemicals and biofuels.

## 1. Introduction

Lignocellulosic biomass represents a crucial renewable resource for the partial or total substitution of conventional raw materials. Numerous studies have demonstrated its potential to be transformed into biofuels, chemicals and high value-added materials capable of replacing products traditionally derived from petrochemical refineries [1,2]. However, the rapid expansion of the global economy has led to an unsustainable accumulation of waste [3], with an estimated 181.5 billion tons of lignocellulosic wastes generated annually [4]. Lignocellulosic biomass primarily consists of cellulose (40–50 %), hemicellulose (25–35 %) and lignin (15–20 %). Due to their complex composition and structure, a wide variety of chemical products of interest can be obtained but are usually reached with poor selectivity [5].

Structurally, lignocellulosic biomass is organized into crystalline and amorphous domains. The crystalline fraction comprises cellulose fibrils, while the amorphous region contains hemicellulose and lignin [6]. Hemicellulose acts as a binding agent, reinforcing the cellulose-hemicellulose-lignin network. [7]. The amorphous lignin heteropolymer, is composed of phenylpropane units (p-coumaryl, coniferyl, and sinapyl alcohol) interconnected by various types of linkages. This amorphous heteropolymer is water-insoluble and optically inactive, making its degradation particularly challenging. [6]. The solubility of lignin in acid, neutral or alkaline environments depends on the monomeric composition of the lignin (p-coumaryl, coniferyl, sinapyl alcohol or combinations of them) [8].

Despite the challenges associated with lignin, the complex structure of this polymer offers a significant opportunity for selective transformation into valuable products. Catalytic methods, particularly those based on metal oxides, have attracted considerable attention due to their

This article is part of a special issue entitled: Biorefineries and Separations published in Biomass and Bioenergy.

* Corresponding author. Chemical & Environmental Engineering Group, Universidad Rey Juan Carlos. C/Tulipán s/n, 28933, Móstoles, Spain.
*E-mail address:* juan.melero@urjc.es (J.A. Melero).

https://doi.org/10.1016/j.biombioe.2025.107936
Received 30 January 2025; Received in revised form 23 April 2025; Accepted 23 April 2025
Available online 1 May 2025

advantages over traditional techniques such as dissolution or pyrolysis-based degradation [9]. Metal oxides, including alkali metal oxides like strontium oxide (SrO), calcium oxide (CaO), barium oxide (BaO), and magnesium oxide (MgO), provide high specific surface areas, adjustable acid-base properties, and reliable performance in biomass depolymerization [9]. NaOH as a homogeneous catalyst has been also widely used for delignification, achieving up to 84.5 % efficiency [10,11], but it presents drawbacks like difficult separation and corrosive environments, which are addressed by basic heterogeneous catalysts, offering easier recovery, lower corrosivity, and sustainable operation.

Among alkali metal oxides, MgO emerges as an effective option, offering high basicity and thermal stability, which allows its application under moderate reaction conditions [12,13]. Previous investigations have demonstrated the potential of MgO for the depolymerization of lignin, reaching lignin removal ratios up to 24 % [14]. This efficiency is increased up to 86 % using further oxidants, such as $H_2O_2$ or $O_2$ [15], or 85 % when MgO was dopped with other metals such as La or Ni [16]. However, a few studies have explored the exclusive use of MgO under moderate conditions without additives. The present study investigates the catalytic performance of MgO synthesized through different methods to optimize its activity and selectivity for lignocellulosic waste depolymerization [17].

The catalytic reactions were performed under moderate conditions (<150 °C), at autogenous pressure, without the use of additional oxidants ($O_2$ or $H_2O_2$), and employing water as the sole solvent without further processing. This approach avoids traditional methods such as pyrolysis and the associated costs. Unlike most bio-oil processing methods, which predominantly target bio-oil production, this research focuses on the selective production of carboxylic acids [18–22]. Carboxylic acids are molecules with high-added value since they are involved in the synthesis of an extensive family of polymers, including polyesters and polyamides [23]. Additionally, carboxylic acids find extensive applications across various industries, such as cosmetic, pharmaceutical, chemical, food, and emerging fields like medical technologies, hydrogen production and bio-oils development [24–29]. Hence, the main objective of this study is to evaluate different MgO-based catalysts for the selective delignification of lignocellulosic waste and the co-production of high-value carboxylic acids. The work aims to determine the relationship between the physicochemical properties and the macroscopic catalytic activity of the catalysts (selective delignification and carboxylic acids production).

## 2. Experimental

### 2.1. Source of lignocellulosic waste

The lignocellulosic waste (LW) was collected from an urban waste treatment facility located in Madrid (Spain), mainly composed of prune and gardening wastes. Before catalytic depolymerization, the biowaste was blended and homogenized by a blade mill and screened to achieve a particle size of less than 10 mm.

### 2.2. Chemicals

Glucose (99.99 %), manose (99.99 %), xylose (99.99 %), arabinose (99.99 %), non-volatile fatty acid standard mix (NVFA) (≥99.99 %), volatile free acid mix (VFA) (≥99.99 %), were purchased from Sigma-Aldrich, Spain. Water (Mili-Q quality, Millipore, Spain) was used as a solvent. MgO materials were prepared by using the proper magnesium precursor and chemicals purchased from Sigma-Aldrich, Spain: Mg $(NO_3)_2{\cdot}6H_2O$ (≥99.99 %), ethylene glycol (≥99 %), $Mg(OH)_2$ (≥99 %), benzoic acid (≥99.5 %), $MgCl_2{\cdot}6H_2O$ (≥99.99 %), NaOH (≥98 %), MgO (≥99.99 %), $Mg(OC_2H_5)_2$ (98 %), ethanol (≥99.8 %) and toluene (≥99.5 %).

### 2.3. Preparation of different MgO-based catalysts

Different MgO-based catalysts were synthesized using distinct synthetic protocol methods as follows:

**MgO (I)** sample was synthesized by the sol-gel method using 8.63 g of the precursor Mg $(NO_3)_2$, 2 mL of ethylene glycol, and 2 mL of water. The mixture was stirred for 30 min at room temperature and afterwards calcined with a temperature ramp of 10 °C/min up to 600 °C and kept at this temperature for an additional 2 h [30].

**MgO (II)** sample was prepared by the direct calcination of commercial Mg $(OH)_2$ using the same thermal program as that of the MgO (I) material [31].

**MgO (III)** sample was synthesized using a hydrothermal method to obtain the Mg $(OH)_2$ precursor. 2.0 g of $MgCl_2$ and 0.12 g of benzoic acid were dissolved in 60 mL water with sonication at room temperature and stirred for 10 min. Then, 20 mL of NaOH solution (2M) was added dropwise to the mixture with a vigorous stirring. The slurry was transferred to a 100 mL autoclave and heated to 180 °C for 24 h. The obtained Mg $(OH)_2$ precursor was washed with deionized water and dried at 80 °C under vacuum overnight after filtration. The MgO material was obtained after calcination of the synthesized Mg $(OH)_2$ with a temperature ramp of 10 °C/min at 500 °C and kept at this temperature for an additional 6 h [32].

**MgO (IV)** sample was synthesized by reconstruction of a commercial MgO. Typically, 500 mg of commercial MgO was boiled in water for 5 h, followed by drying at 120 °C overnight. The obtained Mg $(OH)_2$ precursor was calcined at 500 °C for 6 h under a vacuum system [32].

### 2.4. Characterization techniques for MgO-based catalysts

The presence and identification of crystalline phases of the synthesized catalysts was evaluated by XRD performed in a Philips X'Expert unit using Cu-Kα radiation in the 2θ angle range. The data were collected from 5 to 90° (2θ) with a resolution of 0.02° by using the crystalline refinement with X'Pert HighScore Plus software. Database utilized for the identification of XRD peaks is the Crystallography Open Database, specifically the version designated COD23_HS4. For MgO the reference was COD 96-900-6458 [33].

Textural properties were determined by nitrogen adsorption-desorption isotherms using a Micro Active Tristar Plus II (Micrometrics). The samples were autogassed using a heating rate of 5 °C/min until 87 K, and the desorption was made using a heating rate of 5 °C/min until 300 °C and kept for 3 h. The specific surface area was calculated by the Brunauer-Emmett-Teller method ($S_{BET}$) [34]. The macroporosity of the different samples was evaluated using the Micromeritics Micro-Active AutoPore V9600 through mercury intrusion porosimetry under varying pressures. The Maximum Incremental Intrusion of mercury (MII) and Median Pore Diameter (MPD), defined as the pore diameter at which 50 % of the total mercury intrusion has occurred, were calculated.

Thermal Programmed Desorption of $CO_2$ analysis was performed (TPD-$CO_2$) to determine the amount and relative strength of the basic sites of the MgO-based catalysts. The analysis was carried out in a Micrometrics In-situ Catalyst Characterization system (ICCS) equipped with a micro temperature controller SW48 from Ditel. To condition the sample for the analysis, a pre-treatment of 30 min at 550 °C was first carried out, followed by $CO_2$ adsorption at 100 °C for 30 min. Afterwards, a physical desorption step at 100 °C in a helium atmosphere is performed for 15 min, and finally, the chemical desorption was performed by heating up to 800 °C under helium atmosphere, with a heating ramp of 10 °C/min [35]. During the chemical desorption, the amount of $CO_2$ release with the temperature is monitored to calculate the amount and relative strength of the different basic sites of the MgO materials.

Scanning Electron Microscope (SEM) was carried out to observe the morphology of the samples using the Phenom XL G2 Desktop SEM. Transmission Electron Microscopy (TEM) has been performed to

visualize morphology in more detail together with the estimation of the interplanar distance using the JEM 2100HT.

### 2.5. Catalytic depolymerization tests of lignocellulosic waste

The catalytic reactions were conducted in a multi-reactor (12 plus carousel, Radleys) with 12 positions. Each position consists of a 15 mL glass tube reactor stirred with a magnetic bar. Typically, 0.1 g of the previously dried lignocellulose material was mixed with 20 wt% of catalyst and 5 mL of ultrapure water. The tube was then sealed and placed in the carousel, previously heated to a determined temperature for different reaction times. At the end of the reaction, the solid mixture composed of the non-reacted lignocellulosic solid and the catalyst was separated from the aqueous phase by filtration and then was dried at 110 °C overnight. Afterwards, the catalyst and the unreacted lignocellulose were separated through a sieve with an aperture size of 0.1 mm. The remaining lignocellulosic solid was characterized to monitor the delignification process (see section 3.6) whereas the recovered catalyst is used in a successive catalytic cycle to study its reusability. The composition of the liquid phase was characterized by means of HPLC chromatography (see section 3.6).

### 2.6. Analytical techniques for monitoring catalytic depolymerization of the lignocellulosic waste

The raw lignocellulosic waste and non-reacted lignocellulosic solid resultant of the catalytic hydrothermal depolymerization were characterized by different techniques [36].

X-Ray diffraction analysis (XRD) was carried out with a Philips X' Pert PRO diffractometer (Malvern Panalytical, Netherlands). The XRD spectra were recorded from 0 to $90^0$ (2θ) with a resolution of $0.02^0$ using the Cu-Kα radiation for samples previously dried at 100 °C overnight. The crystallinity index (CrI) of the lignocellulosic solids [37].

$$CrI = \frac{I_{002} - I_{amorphous}}{I_{002}} \times 100 \quad \text{(Eq.1)}$$

Where:

$I_{002}$: maximum intensity of the diffraction peak at $2\theta = 22.5^\circ$ (corresponding to Miller index 002).

$I_{amorphous}$: intensity at $2\theta = 18.7^\circ$.

Scanning electron microscopy (SEM) and Infrared Spectroscopy (IR) were employed to determine the morphology and functional groups of fresh lignocellulosic waste and non-reacted lignocellulosic solids after catalytic hydrotreatment. Scanning electronic microscopy was carried out using a Phenom XL G2 Desktop SEM. Fourier Transform Infrared Spectroscopy FTIR was performed by Attenuated Total Reflectance method (FTIR-ATR) between 400 and 4000 $cm^{-1}$ using a Spectrum 100 system (PerkinElmer, US).

The mass conversion of the lignocellulosic waste was calculated by means of Eq. (2).

$$X\,(\%) = \frac{m^0 - m^f}{m^0} \cdot 100 \quad \text{(Eq 2)}$$

Where:

$m^o$: the initial mass of the lignocellulosic waste.

$m^f$: mass of the resultant solid fraction after the hydrothermal catalytic depolymerization.

Elemental and thermogravimetric analyses were used to monitor the carbon mass conversion as well as the specific conversion of each polymer present in the lignocellulosic residue (cellulose, hemicellulose and lignin). Elemental analysis was conducted using a HCNS-O Flash 2000 analyzer (Thermo Fisher Scientific). The analysis of samples was performed by triplicate and an average value was obtained with its experimental error. The carbon mass conversion was also calculated using carbon elemental analysis data (Eq. (3)).

$$X_c\,(\%) = \frac{m_c^o - m_c^f}{m_c^o} \cdot 100 \quad \text{(Eq. 3)}$$

Where:

$m_c^o$: carbon mass in the fresh lignocellulosic waste.

$m_c^f$: carbon mass in the remaining solid after hydrothermal catalytic treatment.

Thermogravimetric analysis (TGA) using a TGA-DSC1, Mettler-Toledo, S.A.E was used to determine the composition of each lignocellulosic polymer "p" as cellulose, hemicellulose and lignin, according to the previous method described in literature [36]. Details of the temperature program used for the TGA analysis, as well as a typical TGA profile of the fresh lignocellulosic waste are provided in Figure S1 and Figure S2, respectively. In these analyses, an initial small mass loss is observed below 100 °C attributed to the presence of water (ca. less than 5 wt %). A subsequent mass loss at 400 °C is associated with the degradation of cellulose and hemicellulose, while mass losses occurring at 600 °C and above are attributed to lignin decomposition. To accurately determine the weight fraction of each polymer of the solid, the TGA peaks were deconvoluted using the Origin software (Fig. S3), considering the water content and the final solid residue. These weight percentages and the total solid mass allow us to measure the amount of each polymer in the solid ($m_p$) for the fresh residue and the remaining solid fraction after the hydrothermal catalytic treatment. Consequently, the conversion of each polymer ($X_p$) after the hydrothermal catalytic treatment ($X_C$ cellulose, $X_H$ hemicellulose and $X_L$ lignin, respectively) was calculated according to Eq. (4):

$$X_p\,(\%) = \frac{m_p^0 - m_p^f}{m_p^0} \cdot 100 \quad \text{(Eq. 4)}$$

Where:

$m_p^0$: initial mass of the polymer in the fresh lignocellulosic waste.

$m_p^f$: mass of the polymer in the remaining solid after the hydrothermal catalytic treatment.

To monitor the delignification of the solid during the hydrothermal catalytic treatment, a selective lignin removal (SLR) parameter has been defined as follows (Eq. (5))

$$SLR = \frac{m_f^L}{m_f^P} \quad \text{(Eq. 5)}$$

Where:

$m_f{}^L$: converted grams of lignin after the catalytic hydrothermal treatment.

$m_f{}^P$: converted grams of all the polymers (lignin, hemicellulose and cellulose) after catalytic hydrothermal treatment.

The analysis of the aqueous solution after the catalytic hydrothermal depolymerization was carried out by means of High-Performance Liquid Chromatography (HPLC) with an Agilent 1260 Infinity chromatograph equipped with a refractive index (RID) G13662A detector and using a Hi-Plex H column (300 × 7.7 mm) from Phenomenex. Before the analysis, liquid samples were filtered through a cellulose-ester filter of 0.2 μm of pore size. The analyses were performed at 65 °C on the column and using 1 mL/min of 0.005M $H_2SO_4$ as the eluent. The quantified compounds have been grouped in four families: (*i*) monomeric sugars coming from the hydrolysis of cellulose and hemicellulose (*ii*) **VFAs** including formic acid, acetic acid, propanoic acid, butyric acid, isobutyric acid, valeric acid, iso-valeric acid, hexanoic acid and heptanoic acid (iii) **NVFAs** including oxalic acid, oxaloacetic acid, lactic acid, succinic acid, malonic acid, pyruvic acid and fumaric acid and (iv) finally **other compounds** not identified by HPLC (sugar oligomers from carbohydrates, degradation aromatic compounds from lignin and by-products arising from further secondary reactions). In order to monitor the hydrothermal catalytic depolymerization of polymers into soluble organic compounds (sugars, VFAs, NVFAs and other degradation

**Table 1**
Chemical composition of milled-treated feedstock (on dry weight basis).

| Parameter | Value |
|---|---|
| Polymer distribution | |
| Cellulose (wt. %) | 41.7 ± 5 |
| Hemicellulose (wt. %) | 30.8 ± 5 |
| Lignin (wt. %) | 24.2 ± 5 |
| Ash (wt. %) | 3.2 ± 5 |
| Elemental analysis | |
| Hydrogen (wt.%) | 5.8 ± 0.2 |
| Carbon (wt.%) | 59.1 ± 0.5 |
| Nitrogen (wt.%) | <0.1 |
| Sulphur (wt.%) | <0.1 |
| Oxygen (wt.%) | 35.0 ± 0.4 |
| Crystallinity index | |
| CrI (%) | 61.7 |

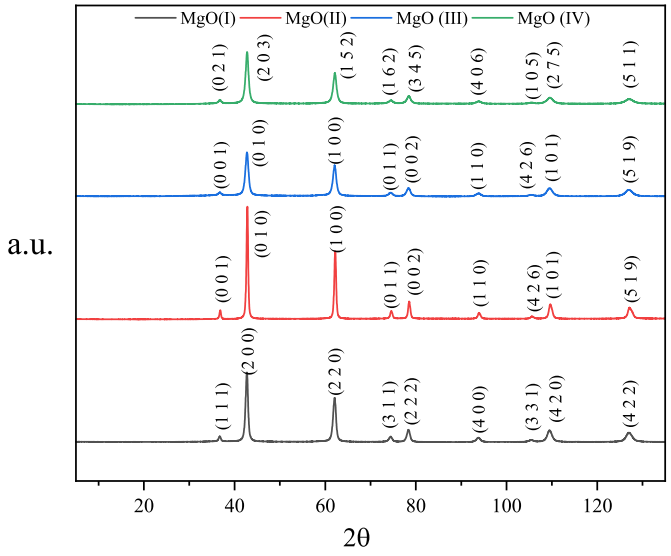


**Fig. 1.** XRD diffractograms of the different MgO synthesized samples.

products), the following parameters were calculated in terms of carbon mass.

- Carbon yield of the compound *i.*

$$Y_i(\%) = \frac{m_c^i}{m_c^0} \cdot 100 \quad \text{(Eq. 6)}$$

Where:
$m_c^i$: mass of carbon transformed into compound i (sugars, NVFAs and VFAs) measured by HPLC.
$m_c^0$: mass of carbon of the initial lignocellulosic waste by HCNOS analysis.

- Carbon selectivity towards the compound i.

$$S_i(\%) = \frac{Y_i}{X_c} \cdot 100 \quad \text{(Eq. 7)}$$

- Carbon selectivity towards other compounds not identified by HPLC.

$$S_{others}(\%) = 100 - \sum S_i(\%) \quad \text{(Eq. 8)}$$

Finally, the aqueous phase after the catalytic hydrothermal depolymerization was also analyzed by ICP-OES to evaluate a partial solubilization of Mg species within the reaction medium during the catalytic reaction.

## 3. Results and discussion

### 3.1. Characterization of the initial lignocellulosic waste

Table 1 summarizes the characterization data of fresh LW in terms of the polymer components, elemental analysis and crystallinity index. The percentage of characteristic polymer domains (cellulose, hemicellulose and lignin) determined by TGA are consistent with typical values reported for lignocellulosic wastes in the literature [38]. Elemental analysis revealed negligible content of N and S, which were lower than the detection limit of the equipment. Interestingly, the LW showed a moderate crystallinity index (CrI) of ca. 62 %, a factor known to critically influence catalytic degradation. High CrI values are associated with reduced accessibility of the lignocellulosic matrix to the active sites of the catalyst, as reported in previous studies [22,39].

### 3.2. Physicochemical characterization of MgO-based catalysts

Fig. 1 shows the XRD pattern of MgO nanoparticles synthesized using the methods described in the experimental section. Key structural parameters, including average crystallite size (estimated using Scherrer's formula), space group, and unit cell volume are summarized in Table 2. The diffraction peaks at 2θ values of 36.7°, 42.7°, 62.1°, 74.4°, and 78.4° correspond to distinct crystallographic planes, which are indexed based on the crystalline structure and indicated in Fig. 1. Additionally, a schematic representation of the unit cells is provided in Fig. S4, constructed using the database allocated in *Materials Project* free software. As clearly shown, the synthesized MgO-based materials exhibit different spatial structures depending on the synthesis method employed. The absence of additional peaks in the XRD pattern confirms the high purity of the synthesized MgO materials.

As shown in Table 2, the synthesis method also significantly affects the crystallite size. The smallest crystallite size is observed for MgO (I) sample synthesized using the sol-gel method, while the largest corresponds to MgO (II) sample synthesized using $Mg(OH)_2$ as a precursor. Other crystalline parameters, such as the unit cell volume, also vary notably depending on the synthesis route. Specifically, the unit cell volume decreases significantly from 74 $Å^3$ for MgO (I) to 47 $Å^3$ for MgO (IV), 31 $Å^3$ for MgO (III), and finally, the lowest value of 29 $Å^3$ for MgO (II). The unit cell volume is directly related with the interaction of the material with substrates; larger volumes generally indicate stronger substrate interactions [40].

The morphology of the materials was studied using FESEM, as shown in Fig. S5–S8. The SEM images reveal clear morphological differences among the materials with macro and mesoporous domains which also correlate with their crystalline structures. In the case of MgO (I), a higher prevalence of hexagonal plates characteristic of cubic crystalline structure were observed (Fig. S5). In contrast, MgO (II) and MgO (III)

**Table 2**
Characterization results of MgO – based materials.

| | Average crystal size (nm) | Crystalline structure/Space group | Volume ($Å^3$) | MPD (nm) | Porosity (%) | MII ($cm^3/g$) | mmol $CO_2/g$ |
|---|---|---|---|---|---|---|---|
| MgO (I) | 12.84 | Cubic/Fm-3m | 74.78 | 4217 | 77.4 | 0.586 | 23.1 |
| MgO (II) | 21.85 | Triclinic/P1 | 29.73 | 2228 | 86.1 | 0.329 | 9.9 |
| MgO (III) | 13.65 | Triclinic/P1 | 31.29 | 125 | 75.1 | 0.235 | 13.5 |
| MgO (IV) | 16.18 | Monoclinic/P1 | 47.75 | 262 | 72.1 | 0.039 | 10.8 |

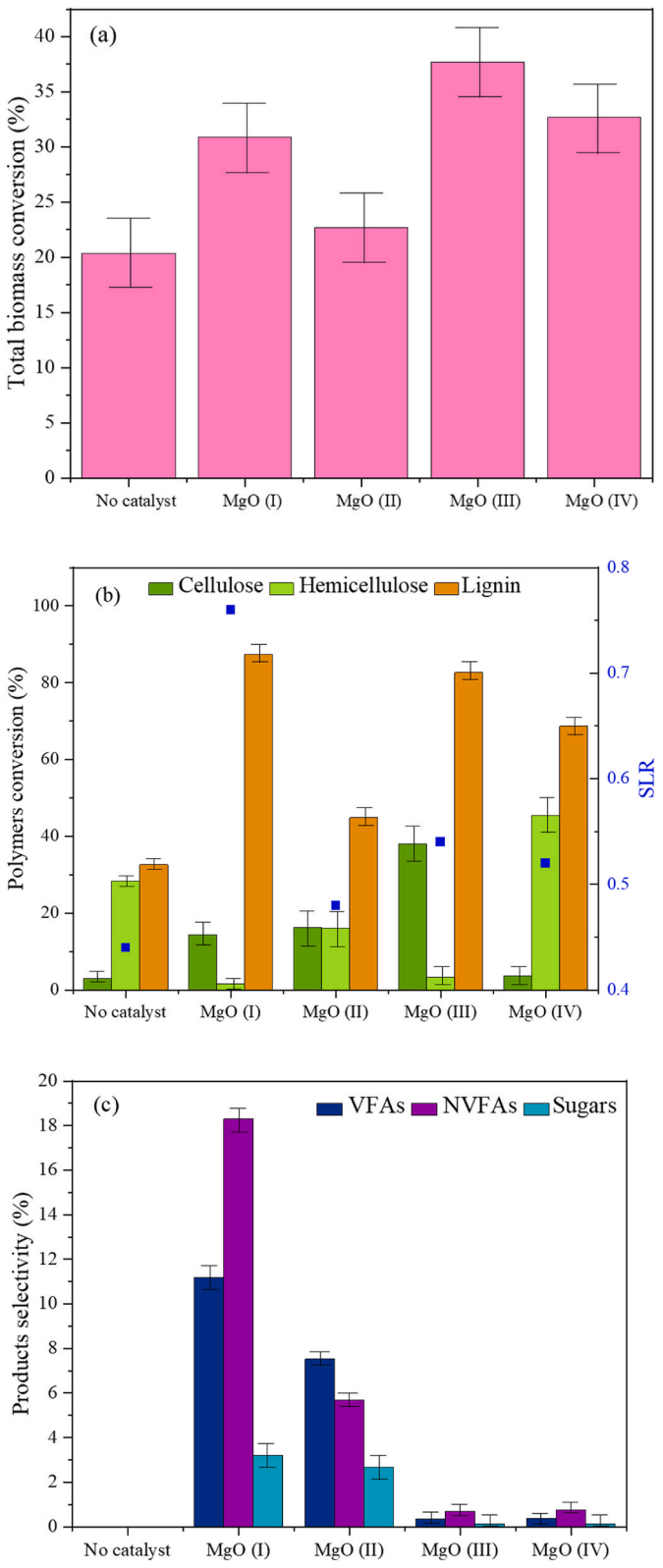


**Fig. 2.** (a) Total biomass conversion. (b) Cellulose, hemicellulose and lignin conversions. (c) Family products in the liquid phase in terms of carbon selectivity. Reaction conditions: 120 min, 120 °C, 20 wt% catalyst loading referred to the LW mass, 0.1 g of LW and 5 mL of $H_2O$.

(Fig. S6 and S7), exhibited more diverse morphologies, including elongated plates associated with triclinic structures. Finally, for the catalyst MgO (IV) (Fig. S8), crystals with a needle-like morphology were observed, consistent with a monoclinic crystalline structure.

Fig. S9 shows the mercury adsorption tests of the different MgO based catalysts. Although porosity values were quite similar, the Maximum Incremental Intrusion of mercury (MII) and Median Pore Diameter (MPD) displayed large differences between all the materials (Table 2). MgO (I) sample depicts the highest MII and MPD values indicating a greater quantity of macropores and larger pore sizes. Additionally, nitrogen adsorption-desorption isotherms were used to further investigate the surface area and the porous characteristics of the synthesized MgO samples (Fig. S10 and S11). All the samples displayed type III isotherms, typical of macroporous materials, according to the IUPAC classification [41].

Fig. S12 shows $CO_2$-TPD desorption profiles [42] whereas the overall basicity values for the different synthesized MgO samples are summarized in Table 2. Basic sites in the temperature range of 45–150 °C are weak in nature and are associated with surface hydroxyl groups. Medium-strength basic sites, attributed to $Mg^{2+}$–$O^{2-}$ pairs, are observed between 150 and 300 °C. Strong basic sites, typically related to low-coordinated oxide species, are detected above 400 °C. The basicity of the samples decreases in the following order: MgO (I) > MgO (III) > MgO (IV) > MgO (II). However, the distribution of basic sites varies significantly depending on the synthesis method. MgO (I) predominantly exhibits medium-strength basic sites (86 %) and also shows the highest absolute basicity (23.1 mmol $CO_2$/g). In contrast, for MgO (II), synthesized from $Mg(OH)_2$, the total basicity drops significantly to 9.9 mmol $CO_2$/g, accompanied by an increase in strong basic sites and a reduction in medium-strength sites.

These characterization results clearly demonstrate that the synthesis method induces significant changes in the structure and base properties of the final materials which might be crucial for their catalytic performance in the hydrothermal catalytic depolymerization reactions.

### 3.3. *Catalytic depolymerization of lignocellulosic waste*

#### 3.3.1. *Screening of the different MgO-based catalysts*

Catalytic hydrothermal depolymerization was performed over the different MgO-based catalysts under selected reaction conditions (120 min, 120 °C, 20 wt% catalyst loading referred to the LW mass, 0.1 g of LW and 5 mL of $H_2O$). Additionally, a blank experiment in the absence of a catalyst was included to evaluate the performance of the hydrothermal treatment at 120 °C as itself. Fig. 2 (a) and (b) show the total biomass and the polymer conversions respectively whereas Fig. 2 (c) displays the percentage of the sugars, VFA and NVFA in the liquid phase (in terms of carbon selectivity) and Table 3 summarizes absolute VFAs and NVFAs concentrations within the aqueous solution.

A variation on the total conversion of LW ranging from 23 % to 38 % was observed depending on MgO-based material (Fig. 2 (a)). Interestingly, the non-catalytic test achieved a total conversion of about 27 %, which is near the value of the less active MgO (II) based materials which reveal that the hydrothermal treatment promotes an important solid conversion of the LW. However, the results regarding the individual cellulose, hemicellulose and lignin removals displayed remarkable differences for the different catalysts and non-catalytic test (Fig. 2 (b)). The hydrothermal treatment in absence of catalyst showed low conversions and non-selective conversion between cellulose, hemicellulose and lignin. The incorporation of MgO-based materials produced a selective enhancement of the lignin conversion, which increased significantly from 38 % up to 90 %. The cellulose and hemicellulose conversions were always lower than the lignin ones and selective conversion of lignin versus cellulose/hemicellulose varied depending on the MgO-based materials. MgO (I) stands out as the most selective catalyst for delignification, achieving cellulose, hemicellulose and lignin conversions of 1.3 %, 22 % and 90 %, respectively, corresponding to a SLR value of 0.76

**Table 3**
Carboxylic acids concentration after hydrothermal catalytic treatment over MgO based catalysts. Reaction conditions: 120 min, 120 °C, 20 wt% catalyst loading referred to the LW mass, 0.1 g of LW and 5 mL of $H_2O$.

| Concentration (g/L) | No catalysts | MgO (I) | MgO (II) | MgO (III) | MgO (IV) |
|---|---|---|---|---|---|
| Succinic acid | 0.00 | 0.08 | 0.00 | 0.00 | 0.00 |
| Fumaric acid | 0.00 | 0.97 | 0.00 | 0.00 | 0.00 |
| Pyruvic acid | 0.00 | 0.82 | 0.00 | 0.00 | 0.00 |
| Lactic acid | 0.00 | 0.15 | 0.10 | 0.06 | 0.06 |
| Oxalic acid | 0.00 | 0.77 | 0.07 | 0.03 | 0.03 |
| Oxalacetic acid | 0.00 | 0.00 | 0.47 | 0.00 | 0.00 |
| Malonic acid | 0.00 | 0.00 | 0.14 | 0.01 | 0.01 |
| **Total NVFAs** | 0.00 | **2.78** | **0.78** | **0.10** | **0.11** |
| Formic acid | 0.00 | 0.52 | 0.32 | 0.02 | 0.02 |
| Acetic acid | 0.00 | 1.00 | 0.58 | 0.04 | 0.04 |
| Propionic acid | 0.00 | 0.19 | 0.02 | 0.00 | 0.00 |
| Isobutyric acid | 0.00 | 0.00 | 0.00 | 0.00 | 0.00 |
| Butyric acid | 0.00 | 0.00 | 0.00 | 0.00 | 0.00 |
| Hexanoic acid | 0.00 | 0.00 | 0.00 | 0.00 | 0.00 |
| Heptanoic acid | 0.00 | 0.00 | 0.04 | 0.00 | 0.00 |
| **Total VFAs** | 0.00 | **1.71** | **0.96** | **0.06** | **0.06** |

(indicating that 76 % of the converted polymers is lignin). In contrast, the blank catalytic run and the rest of the catalyst showed a lower selective delignification as reflected by significantly lower SLR values.

The lignin in the LW contains many functional groups such as hydroxyl groups, carboxyl groups and aromatic rings. Since all the reactions took place in neutral water, the ionization of the carboxylic groups resulted in a negative charge on the lignin. In fact, the literature reports a zeta potential of lignin at neutral pH of −21.87 mV [43], while under the same pH conditions, MgO has a positive surface charge [44]. Therefore, attractive electrostatic interactions occur between the LW and the MgO surface. Furthermore, the cationic interactions between $Mg^{2+}$ and LW strengthen these binding forces, facilitating the depolymerization of the lignin fraction [43,45]. This would explain the selective depolymerization of the lignin that makes up the LW.

The reaction aqueous phase was evaluated by ICP-OES to verify that none of the tested catalysts underwent significant dissolution into the reaction medium during the catalytic reaction. The Mg leaching was found to be below 2 % for all the catalyst tested (MgO (I) 1.01 %, MgO (II) 1.56 %, MgO (III) 1.67 % and MgO (IV) 1.67 %), confirming the stability of the catalysts under the hydrothermal reaction conditions [46]. This negligible leaching may also explain the slight increase of the pH up to 9.5 after the catalytic process.

Regarding the analysis of the family products analyzed in the liquid phase after the catalytic depolymerization reactions (Fig. 2 (c)), the catalyst that resulted in a better performance was also the MgO (I) material, with a carbon selectivity of 11.2 %, 18.3 % and 3.2 % of VFAs, NVFAs and sugars, respectively (that means ca. 30 % of the carbon in the initial LW is transformed into marketable carboxylic acids). It must be noteworthy the high production of (di) carboxylic acids in NVFA group for this material as one of the important achievements of an effective catalytic depolymerization of LW (Table 3). MgO (I) gave an interesting mixture formed by oxalic, fumaric and pyruvic acids in approximately the same concentration. MgO (I) produced the highest quantity of fumaric acid, which is among the acids with a major value as a pharmaceutically active substance and in the production of polyester resins [47]. The other MgO-based materials yielded a significant lower production of VFAs and NVFAs.

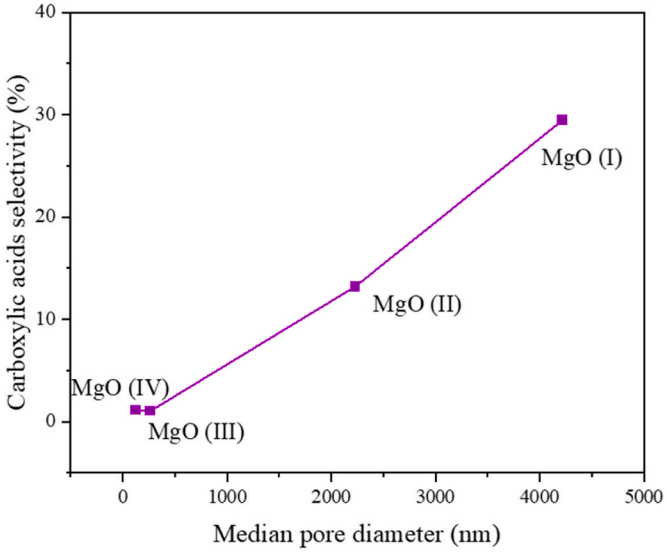


**Fig. 3.** Carbon selectivity towards carboxylic acids (%) *vs* median pore diameter (nm) of the different MgO based catalysts.

Finally, the catalytic performance of the MgO-based materials was correlated with specific parameters obtained from the physicochemical characterization. The highest selective lignin removal was achieved for MgO (I) sample, far from those values obtaining for the rest of the MgO materials. This behavior appears to be associated with the combination of medium-strength basicity and extensive macroporosity. MgO (I) exhibited the highest density of medium-strength basic sites (Fig. S12),

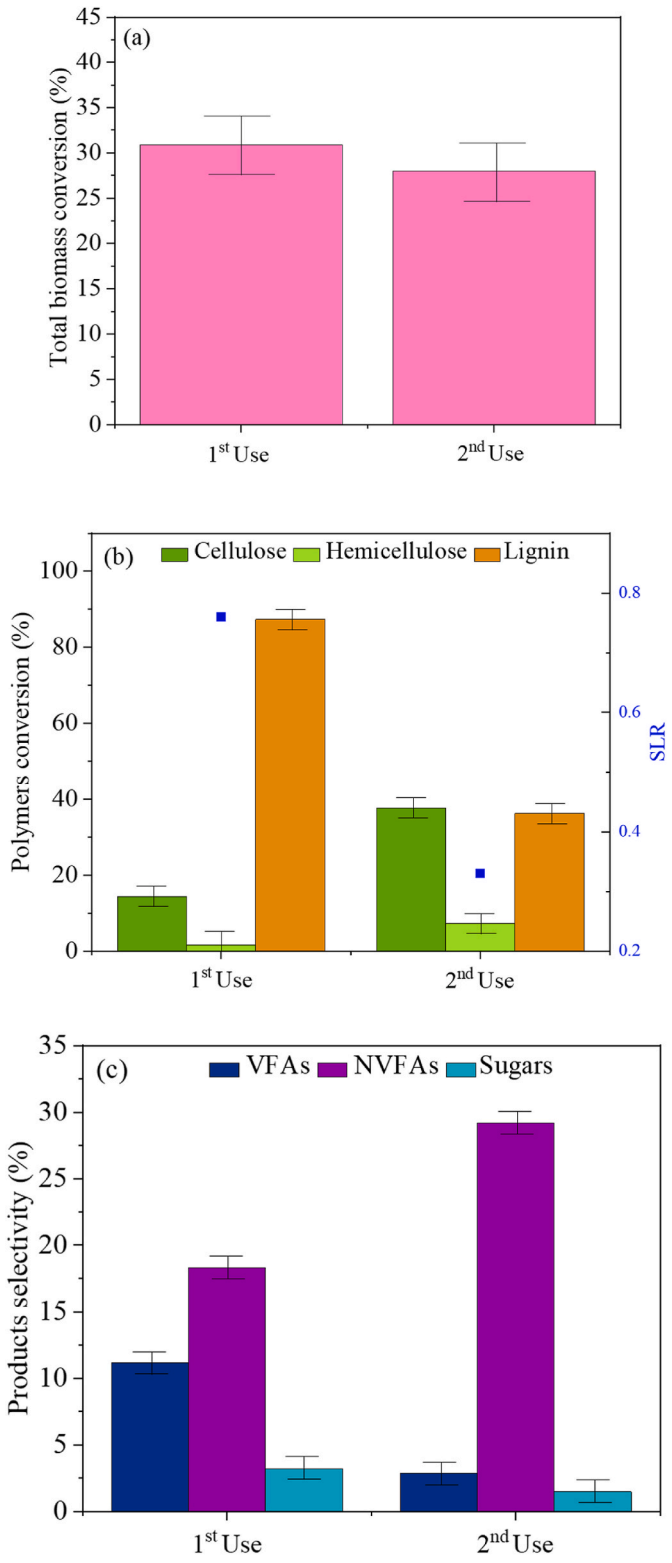


**Fig. 4.** (a) Total biomass conversion. (b) Cellulose, hemicellulose and lignin conversions. (c) Family products in the liquid phase in terms of carbon selectivity. Reaction conditions: MgO (I) as catalyst, 120 min, 120 °C, 20 wt% catalyst loading referred to the LW mass, 0.1 g of LW and 5 mL of $H_2O$.

likely responsible for its selective delignification capability, as well as the highest degree of macroporosity (Table 2), which enhances lignin accessibility to the active sites. Although MgO (II) showed significant macroporosity, its lower overall density of basic sites seems to limit both biomass conversion and subsequent carboxylic acid production. For MgO (III) and MgO (IV), the intermediate basicity values coupled with reduced macroporosity resulted in a less selective lignin conversion of the lignocellulosic waste. Notably, macroporosity appears to play a key role in promoting the production of carboxylic acids. As shown in Fig. 3, a linear correlation was observed between the carbon selectivity towards carboxylic acid production and the median pore diameter obtained from mercury intrusion porosimetry. Additionally, it was evident that a higher proportion of strong basic sites promotes the depolymerization of cellulose and hemicellulose, as exemplified by MgO (IV), which achieved a hemicellulose conversion of approximately 50 %.

### 3.3.2. *Effect of temperature and reaction time in the catalytic performance of MgO (I)*

Due to the high selectivity on lignin conversion and the high selectivity towards the products of interest, the most adequate catalyst to selectively transform lignin polymer into products of interest is MgO (I). Thus, the influence of temperature and the kinetics over this MgO (I) catalyst was further evaluated.

The effect of temperature was studied in the range of 100–140 °C. Fig. S13 and Table S1 show the conversion results using MgO (I) as catalyst after 120 min of reaction. When examining the total solid and lignin conversion, no significant difference is observed with varying reaction temperatures but 120 °C allows a better selective removal of the lignin. However, the carbon selectivity toward carboxylic acids increases as temperature rose from 100 °C to 120 °C, indicating that higher temperatures favor the depolymerization towards the formation of valuable products. In contrast, increasing the temperature further up to 140 °C leads to the decrease of NVFA and VFA products in the aqueous effluent. Therefore, under the tested reaction conditions the optimal temperature for promoting a higher production of carboxylic acids is 120 °C.

Fig. S14 shows the results of the reaction kinetics of the MgO (I) tested at 120 °C, where it can be observed that, from the early beginning, the reaction exhibited high selectivity toward lignin conversion, with SLR values over 0.75. On the other hand, the production of carboxylic acids increases significantly after 30 min of reaction and thereafter decreases gradually due to the transformation of the previously formed carboxylic acids to other compounds induced for secondary reactions. It must be noted that just 30 min of reaction can be considered as an optimum value to maximize the production of carboxylic acids. Therefore, treatment intensity (temperature and time) must be controlled to carry out a selective delignification accompanied by an optimum production of carboxylic acids.

### 3.3.3. *Catalyst stability of MgO (I)*

Finally, MgO (I) catalyst was reused in two additional catalytic runs at 120 °C to check its stability. Fig. 4 (a) and (b) show the total solid and polymers conversions for the MgO (I) catalyst after two uses. It was observed that the catalyst loses the selective degradation of the lignin after the reuse with a significant decrease of SLR parameter. Table 4 shows how the concentration of NVFAs type products changes practically from the second use where a large amount of oxalacetic acid was observed. Regarding the distribution of VFAs, note that as the catalyst was reused, more formic acid and less acetic acid were produced.

To justify the different catalytic performance of the MgO catalysts in the second catalytic run, the recovered catalyst after the first catalytic run was characterized. Fig. S15 (a) shows the XRD of the recovered catalyst in comparison with the fresh one where a diffraction pattern corresponding to the formation of Mg $(OH)_2$ is clearly observed. The Mg $(OH)_2$ formation must be attributed to the hydrothermal conditions of the reaction [48]. Moreover, this change in the XRD diffraction pattern is corroborated by the $CO_2$ TPD analysis (Figure S15 (b)) where strong basic sites arising from the Mg $(OH)_2$ formation are clearly evidenced accompanied with the decrease of medium basic sites that were predominant in the fresh MgO (I) sample. The formation of these strong

**Table 4**
Final NVFAs and VFAs concentration (g/L) of catalyst after different catalytic cycles.

| Concentration (g/L) | 1st Use | 2nd Use |
|---|---|---|
| Succinic acid | 0.08 | 0.37 |
| Fumaric acid | 0.97 | 0.00 |
| Pyruvic acid | 0.82 | 0.00 |
| Lactic acid | 0.15 | 0.05 |
| Oxalic acid | 0.77 | 0.30 |
| Oxalacetic acid | 0.00 | 3.10 |
| Malonic acid | 0.00 | 0.00 |
| **Total NVFAs** | **2.78** | **3.82** |
| Formic acid | 0.52 | 0.33 |
| Acetic acid | 1.00 | 0.04 |
| Propionic acid | 0.19 | 0.01 |
| Isobutyric acid | 0.00 | 0.10 |
| Butyric acid | 0.00 | 0.01 |
| Valeric acid | 0.00 | 0.00 |
| Hexanoic acid | 0.00 | 0.00 |
| Heptanoic acid | 0.00 | 0.00 |
| **Total VFAs** | **1.71** | **0.47** |

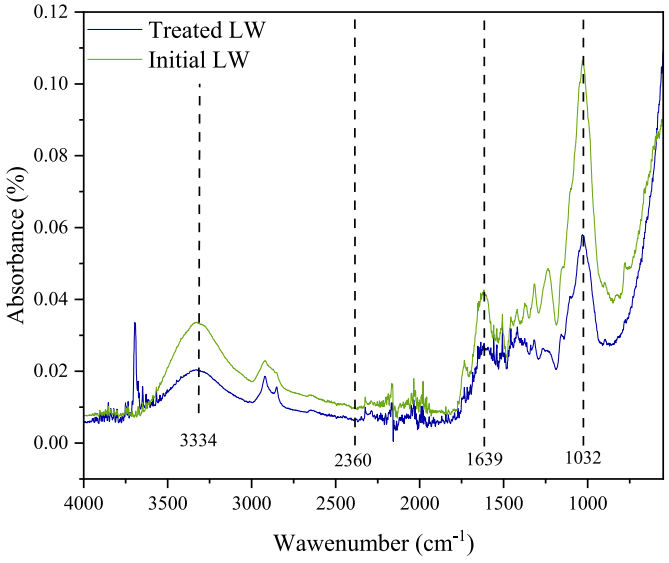


**Fig. 5.** FTIR spectra of LW before and after catalytic treatment with MgO (I).

basic sites would explain the change in the catalytic performance. Therefore, further efforts should be directed toward modifying the MgO (I) catalyst to enhance its stability under reaction conditions.

Finally, the changes suffered by LW after catalytic hydrothermal treatment have been elucidated by means of FTIR (Fig. 5). FTIR shows a peak around 1032 $cm^{-1}$ corresponded to aromatic C-H stretching (present in lignin). The band at 1639 $cm^{-1}$ corresponded to aromatic ring (present in lignin) and the band at 2360 $cm^{-1}$ corresponded to C-H stretching of the lignin polymer. The O-H stretching of lignin and hemicellulose polymers was represented by the bands around 3318 and 3815 $cm^{-1}$ [49]. All relative band intensities were reduced after the catalytic treatment with MgO (I), an indication of degradation of lignin polymer during the treatment. The reduction in relative intensity is a strong indication of the cleavage of lignin side chains [49]. XRD spectra comparing fresh LW and pretreated LW (Fig. S16) shows an increase of the crystallinity index (CrI) from 61.7 % to 70.9 %. The increase in CrI was caused by the removal of amorphous substances in the biomass, mostly lignin, which exposed the crystalline cellulose core [50]. These changes after catalytic treatment are also clearly observed in the SEM images (Fig. S17). Prior to the catalytic hydrotreatment, the outermost layers of lignin envelop the inner layers of cellulose and hemicellulose fibres (Figure S17 (a)) but after catalytic treatment (Figure S17 (b)) the lignin was detached, thereby exposing the cellulose and hemicellulose fibres.

## 4. Conclusions

Catalytic results show that the strength and density of basic sites as well as the macroporosity of the synthesized MgO materials are crucial in the catalytic performance. The MgO (I) catalyst prepared by a solgel method and characterized by a highly developed macroporous structure and a predominance of medium-strength basic sites, showed the best

catalytic performance in terms of selective lignin depolymerization and production of carboxylic acids as valuable products. These results were achieved under mild reactions conditions (120 °C) and using water as a solvent in absence of any additional oxidant. Under the optimized reaction conditions, 76 % of the converted polymers corresponded to the lignin fraction (SLR ca. 0.76) and over 30 % of the converted carbon of the lignocellulosic waste is transformed into marketable carboxylic acids (in special dicarboxylic acids), being values comparable to those achieved in acidogenic fermentation processes. Further research is still needed to prevent magnesium hydroxide formation and maintain catalytic performance over successive reaction cycles.

## CRediT authorship contribution statement

**N. Vidal:** Writing – original draft, Methodology, Investigation, Data curation. **M. Ventura:** Writing – review & editing, Supervision, Methodology, Investigation, Data curation, Conceptualization. **M. Orfila:** Methodology, Investigation, Data curation. **F. Martínez:** Writing – review & editing, Validation, Supervision, Methodology, Conceptualization. **J.A. Melero:** Writing – review & editing, Validation, Supervision, Methodology, Funding acquisition, Formal analysis, Data curation, Conceptualization.

## Acknowledgements

PID2021-122334OB-I00 (SAFADCAT), a project funded by MICIN/AEI/10.13039/501100011033/FEDER, UE, is gratefully acknowledged.

## Appendix A. Supplementary data

Supplementary data to this article can be found online at https://doi.org/10.1016/j.biombioe.2025.107936.

## Data availability

Data will be made available on request.

## References

[1] L. Xu, S.J. Zhang, C. Zhong, B.Z. Li, Y.J. Yuan, Alkali-based pretreatment-facilitated lignin valorization: a review, Am. Chem. Soc. (2020), https://doi.org/10.1021/acs.iecr.0c01456. Sep. 30.
[2] V. Ashokkumar, et al., Recent advances in lignocellulosic biomass for biofuels and value-added bioproducts - a critical review, Bioresour. Technol. 344 (Jan. 2022) 126195, https://doi.org/10.1016/J.BIORTECH.2021.126195.
[3] F. Fava, et al., Biowaste biorefinery in Europe: opportunities and research & development needs, N. Biotech. 32 (1) (Jan. 2015) 100–108, https://doi.org/10.1016/j.nbt.2013.11.003.
[4] N. Dahmen, I. Lewandowski, S. Zibek, A. Weidtmann, Integrated lignocellulosic value chains in a growing bioeconomy: status quo and perspectives, GCB Bioenergy 11 (1) (Jan. 2019) 107–117, https://doi.org/10.1111/gcbb.12586.
[5] E.B. Vea, D. Romeo, M. Thomsen, Biowaste valorisation in a future circular bioeconomy, in: Procedia CIRP, Elsevier B.V., 2018, pp. 591–596, https://doi.org/10.1016/j.procir.2017.11.062.
[6] A.T.W.M. Hendriks, G. Zeeman, Pretreatments to Enhance the Digestibility of Lignocellulosic Biomass, Elsevier Ltd., Jan. 01, 2009, https://doi.org/10.1016/j.biortech.2008.05.027.
[7] L. Laureano-Perez, F. Teymouri, H. Alizadeh, B.E. Dale, Understanding Factors that Limit Enzymatic Hydrolysis of Biomass Characterization of Pretreated Corn Stover, 2005, https://doi.org/10.1385/ABAB:124:1-3:1081.
[8] J.H. Grabber, How do lignin composition, structure, and cross-linking affect degradability? A review of cell wall model studies, Crop Sci. (May 2005) 820–831, https://doi.org/10.2135/cropsci2004.0191.
[9] M. Ventura, A. Marinas, M.E. Domine, Catalytic processes for biomass-derived platform molecules valorisation, Top. Catal. 63 (9–10) (Sep. 2020) 846–865, https://doi.org/10.1007/s11244-020-01309-9.
[10] W. Jung, D. Savithri, R. Sharma-Shivappa, P. Kolar, Changes in lignin chemistry of switchgrass due to delignification by sodium hydroxide pretreatment, Energies 11 (2) (Feb. 2018), https://doi.org/10.3390/en11020376.
[11] N. Ameram, et al., Chemical Composition in Sugarcane Bagasse: Delignification with Sodium Hydroxide, 2019, https://doi.org/10.11113/mjfas.v15n2.1118.
[12] A.A. Refaat, Biodiesel production using solid metal oxide catalysts, Int. J. Environ. Sci. Tech 8 (1) (2011) 203–221.
[13] N. Oueda, Y.L. Bonzi-Coulibaly, I.W.K. Ouédraogo, Deactivation processes, regeneration conditions and reusability performance of CaO or MgO based catalysts used for biodiesel production—a review, Mater. Sci. Appl. 8 (1) (2017) 94–122, https://doi.org/10.4236/msa.2017.81007.
[14] K. Ye, Y. Tang, D. Fu, T. Chen, M. Li, Effect of magnesium oxide pretreatment on the delignification and enzymatic hydrolysis of corncob, Ind. Crops Prod. 161 (Mar) (2021), https://doi.org/10.1016/j.indcrop.2020.113170.
[15] Q. Yang, J. Shi, L. Lin, L. Peng, J. Zhuang, Characterization of changes of lignin structure in the processes of cooking with solid alkali and different active oxygen, Bioresour. Technol. 123 (Nov. 2012) 49–54, https://doi.org/10.1016/j.biortech.2012.07.070.
[16] H. Li, X. Zheng, H. Zhang, X. Li, J. Long, Selective cleavage of ester linkages in lignin catalyzed by La-doped Ni/MgO, ACS Sustain. Chem. Eng. 8 (41) (Oct. 2020) 15685–15695, https://doi.org/10.1021/acssuschemeng.0c05360.
[17] C.R. Patil, C.V. Rode, Selective production of furanic ethers from lignocellulosic biomass over mesoporous Zr-incorporated SBA-15 catalyst, ChemistrySelect 3 (44) (Nov. 2018) 12504–12511, https://doi.org/10.1002/slct.201801939.
[18] E. Pütün, Catalytic pyrolysis of biomass: effects of pyrolysis temperature, sweeping gas flow rate and MgO catalyst, Energy 35 (7) (2010) 2761–2766, https://doi.org/10.1016/j.energy.2010.02.024.
[19] L. Santamaria, et al., Effect of CeO2 and MgO promoters on the performance of a Ni/Al2O3 catalyst in the steam reforming of biomass pyrolysis volatiles, Fuel Process. Technol. 198 (Feb) (2020), https://doi.org/10.1016/j.fuproc.2019.106223.
[20] E. Huo, et al., Phenols production form Douglas fir catalytic pyrolysis with MgO and biomass-derived activated carbon catalysts, Energy 199 (May 2020), https://doi.org/10.1016/j.energy.2020.117459.
[21] S.D. Stefanidis, et al., Natural magnesium oxide (MgO) catalysts: a cost-effective sustainable alternative to acid zeolites for the in situ upgrading of biomass fast pyrolysis oil, Appl. Catal., B 196 (Nov. 2016) 155–173, https://doi.org/10.1016/j.apcatb.2016.05.031.
[22] M. Ventura, D. Puyol, J.A. Melero, The synergy of catalysis and biotechnology as a tool to modulate the composition of biopolymers (polyhydroxyalkanoates) with lignocellulosic wastes, Catal. Today 397–399 (Aug. 2022) 220–231, https://doi.org/10.1016/j.cattod.2021.09.032.
[23] J. Iglesias, I. Martínez-Salazar, P. Maireles-Torres, D. Martin Alonso, R. Mariscal, M. López Granados, Advances in Catalytic Routes for the Production of Carboxylic Acids from Biomass: A Step Forward for Sustainable Polymers, Royal Society of Chemistry, 2020, https://doi.org/10.1039/d0cs00177e. Aug. 21.
[24] D. Pal, A. Keshav, B. Mazumdar, A. Kumar, H. Uslu, Production and Recovery of Pyruvic Acid: Recent Advances, Springer India, Dec. 01, 2017, https://doi.org/10.1007/s40034-017-0101-4.
[25] J.L. Martín-Espejo, J. Gandara-Loe, J.A. Odriozola, T.R. Reina, L. Pastor-Pérez, Sustainable Routes for Acetic Acid Production: Traditional Processes vs a Low-Carbon, Biogas-Based Strategy, Elsevier B.V., Sep. 20, 2022, https://doi.org/10.1016/j.scitotenv.2022.156663.
[26] D.A. Bulushev, J.R.H. Ross, Towards Sustainable Production of Formic Acid, Wiley-VCH Verlag, Mar. 09, 2018, https://doi.org/10.1002/cssc.201702075.
[27] E. Schuler, M. Demetriou, N.R. Shiju, G.J.M. Gruter, Towards Sustainable Oxalic Acid from CO2 and Biomass, John Wiley and Sons Inc, Sep. 20, 2021, https://doi.org/10.1002/cssc.202101272.
[28] A.K. Jha, et al., A review on bio-butyric acid production and its optimization, Int. J. Agric. Biol. 16 (2014) 1019–1024 [Online]. Available: http://www.fspublishers.org.
[29] A. Komesu, J. Allan Rocha de Oliveira, L. Helena da Silva Martins, M. Regina Wolf Maciel, R. Maciel Filho, Lactic Acid Manufacture, 2017, https://doi.org/10.15376/biores.12.2.Komesu.
[30] S. Li, Combustion synthesis of porous MgO and its adsorption properties, Int. J. Integrated Care 10 (1) (Mar. 2019) 89–96, https://doi.org/10.1007/s40090-019-0174-7.
[31] M. Kitagawa, S. Misu, J. Ichikawa, H. Matsuhashi, Preparation of active MgO by short-time thermal decomposition of Mg(OH)2, Res. Chem. Intermed. 41 (12) (Dec. 2015) 9463–9473, https://doi.org/10.1007/s11164-015-1971-z.
[32] H. Fang, et al., Dispersed surface Ru ensembles on MgO(111) for catalytic ammonia decomposition, Nat. Commun. 14 (1) (Dec. 2023), https://doi.org/10.1038/s41467-023-36339-w.
[33] L.S. Dubrovinsky, S.K. Saxena, Thermal Expansion of Periclase (MgO) and Tungsten (W) to Melting Temperatures, Springer-Verlag, 1997, https://doi.org/10.1007/s002690050070.
[34] Stephen Brunauer, P.H. Emmett, Edward Teller, Adsorption of gases in multimolecular layers, J. Am. Chem. Soc. 60 (2) (1938) 309–319, https://doi.org/10.1021/ja01269a023.
[35] D. Cornu, H. Guesmi, J.M. Krafft, H. Lauron-Pernot, Lewis acido-basic interactions between CO 2 and MgO surface: DFT and DRIFT approaches, J. Phys. Chem. C 116 (11) (Mar. 2012) 6645–6654, https://doi.org/10.1021/jp211171t.
[36] J.F. Saldarriaga, R. Aguado, A. Pablos, M. Amutio, M. Olazar, J. Bilbao, Fast characterization of biomass fuels by thermogravimetric analysis (TGA), Fuel 140 (Jan. 2015) 744–751, https://doi.org/10.1016/j.fuel.2014.10.024.
[37] S. Park, J.O. Baker, M.E. Himmel, P.A. Parilla, D.K. Johnson, Open Access RESEARCH Cellulose crystallinity index: measurement techniques and their impact on interpreting cellulase performance. http://www.biotechnologyforbiofuels.com/content/3/1/10, 2010.
[38] J.A. Okolie, S. Nanda, A.K. Dalai, J.A. Kozinski, Chemistry and Specialty Industrial Applications of Lignocellulosic Biomass', May 01, Springer Science and Business Media B.V, 2021, https://doi.org/10.1007/s12649-020-01123-0.

[39] J. Zhang, et al., Conversion of lignocellulose into biochar and furfural through boron complexation and esterification reactions, Bioresour. Technol. 312 (Sep. 2020) 123586, https://doi.org/10.1016/J.BIORTECH.2020.123586.
[40] P. Bonazzi, L. Bindi, A Crystallographic Review of Arsenic Sulfides: Effects of Chemical Variations and Changes Induced by Exposure to Light, 2008, https://doi.org/10.1524/zkri.2008.0011.
[41] J. Rouquerol, D. Avnir, C.W. Fairbridge, D.H. Everett, J.M. Haynes, N. Pernicone, J. D.F. Ramsay, K.S.W. Sing, K.K. Unger, Recommendations for the characterization of porous solids (Technical Report), Pure Appl. Chem. 66 (8) (1994) 1739–1758, https://doi.org/10.1351/pac199466081739.
[42] T. Selvamani, A. Sinhamahapatra, D. Bhattacharjya, I. Mukhopadhyay, Rectangular MgO microsheets with strong catalytic activity, Mater. Chem. Phys. 129 (3) (Oct. 2011) 853–861, https://doi.org/10.1016/j.matchemphys.2011.05.055.
[43] J. Wang, Y. Qian, Y. Deng, D. Liu, H. Li, X. Qiu, Probing the interactions between lignin and inorganic oxides using atomic force microscopy, Appl. Surf. Sci. 390 (Dec. 2016) 617–622, https://doi.org/10.1016/j.apsusc.2016.08.161.
[44] George A. Parks, The isoelectric points of solid oxides, solid hydroxides, and aqueous hydroxo complex systems, Chem. Rev. 65 (1965), https://doi.org/10.1021/cr60234a002.
[45] R. Li, D. Yang, W. Guo, X. Qiu, The adsorption and dispersing mechanisms of sodium lignosulfonate on Al2O3 particles in aqueous solution, Holzforschung 67 (4) (May 2013) 387–394, https://doi.org/10.1515/hf-2012-0108.
[46] N. Park, H. Chang, Y. Jang, H. Lim, J. Jung, W. Kim, Prediction of adequate pH and Mg2+ dosage using an empirical MgO solubility model for struvite crystallization, Environ. Technol. Innov. 21 (Feb) (2021), https://doi.org/10.1016/j.eti.2020.101347.
[47] P. Yadav, A.K. Chauhan, R.B. Singh, S. Khan, G. Halabi, Organic Acids: Microbial Sources, Production, and Applications, Functional Foods and Nutraceuticals in Metabolic and Non-communicable Diseases, Jan. 2022, pp. 325–337, https://doi.org/10.1016/B978-0-12-819815-5.00053-7.
[48] Y. Jiang, et al., Chemical structure change of magnesium oxide in the wet oxidation delignification process of biomass with solid alkali, ChemCatChem 9 (13) (Jul. 2017) 2544–2549, https://doi.org/10.1002/cctc.201700155.
[49] S. Sharma, V. Sharma, A. Kuila, Cellulase production using natural medium and its application on enzymatic hydrolysis of thermo chemically pretreated biomass, 3 Biotech 6 (2) (Dec. 2016), https://doi.org/10.1007/s13205-016-0465-z.
[50] R. Evans, R.H. Newman, U.C. Roick, I.D. Suckling, A.P.A. Wallis, Changes in Cellulose Crystallinity during Kraft Pulping. Comparison of Infrared, X-Ray Diffraction and Solid State NMR Results', 1995, https://doi.org/10.1515/hfsg.1995.49.6.498.